Desalination and Water Treatment
www.deswater.com

doi: 10.5004/dwt.2017.21184

81 (2017) 209–215
June

Single-step solvothermal synthesis of boron-doped Bi_2WO_6 visible-light-induced photocatalyst and determination of surface characteristics and photocatalytic activities

Chao-Yin Kuo[a], Chung-Hsin Wu[b,*], Ming-Ju Hsu[b]

[a]*Department of Environmental and Safety Engineering, National Yunlin University of Science and Technology, Yunlin, Taiwan, Tel. +886 5 5347311; email: kuocyr@ms35.hinet.net*
[b]*Department of Chemical and Materials Engineering, National Kaohsiung University of Applied Sciences, 415 Chien Kung Road, Kaohsiung, Taiwan, Tel. +886 7 3814526; Fax: +886 7 3830674; email: wuch@kuas.edu.tw (C.-H. Wu), Tel. +886 938152172; email: chute514@gmail.com (M.-J. Hsu)*

Received 9 April 2017; Accepted 4 July 2017

ABSTRACT

A single-step solvothermal method is utilized to synthesize boron-doped Bi_2WO_6 (BBW). Boric acid was the source of the boron dopant and the doped B/W molar ratio was 0.25. The surface characteristics of Bi_2WO_6 (BW) and BBW were elucidated by scanning electron microscopy, transmission electron microscopy, X-ray diffractometry, specific surface area analysis, zeta potential analysis, UV–Vis spectrophotometry, X-ray photoelectron spectroscopy and fluorescence spectrophotometry. C.I. Reactive Red 2 (RR2) was used as the parent compound in evaluating the photocatalytic activity of BW and BBW. The specific surface area, pore volume, band gap and pH of zero point charge of BBW were 84.5 m^2/g, 0.22 cm^3/g, 3.1 eV and 3.7, respectively. The rates of RR2 removal by BW and BBW under irradiation by sunlight and visible light both followed a pseudo-first-order kinetic model. The RR2 photodegradation rate constants of sunlight/BW, visible light/BW, sunlight/BBW and visible-light/BBW system were 3.34, 0.14, 6.19 and 3.44 hr^{-1}, respectively. Boron doping in BW increases its ability to adsorb RR2 and the amount of hydroxyl groups on its surface. Additionally, boron doping in BW enhanced its charge separation efficiency and suppressed the recombination of electron–hole pairs; accordingly, the photocatalytic activity of BBW exceeded that of BW. This study suggested that photo-generated holes played a major role and superoxide radicals played a minor role in the photodegradation of RR2 in sunlight/BBW system.

Keywords: Solvothermal; Bismuth tungstate; Boron; Visible light; Photocatalysis

1. Introduction

Photocatalysis has great potential for efficiently and completely eliminating toxic chemicals from wastewater. As a green chemical technique, photocatalysis is not only cost-effective but also a promising alternative to the use of solar energy. Among the novel photocatalysts, multicomponent metal oxides that contain bismuth are excellent visible-light-activated photocatalysts. Bi_2WO_6 has attracted considerable attention in this respect. Bi_2WO_6 is chemically and thermally stable and non-toxic. However, the rapid recombination of photo-induced electron–hole pairs in Bi_2WO_6 presents a challenge to its practical application [1,2]. To solve this problem, metal [3–6] and non-metal [7–10] doping and coupling with other photocatalysts [1,2,11,12] have been carried out to improve the photocatalytic activity of Bi_2WO_6. These strategies can extend the lifetime of photo-induced electron–hole pairs, increase the surface area, reduce the band gap or increase the range of spectral absorption.

With respect to the coupling of Bi_2WO_6 with photocatalyst, Ju et al. [2] used a hydrothermal process that was followed by

* Corresponding author.

calcination (873 K) to synthesize the $BiVO_4/Bi_2WO_6$ heterojunction photocatalyst. The enhanced photocatalytic activity of $BiVO_4/Bi_2WO_6$ is attributable mainly to the effective separation of photo-induced electron–hole pairs at the interface of the heterojunction. The widened photoabsorption range and improved crystallinity also favor excellent photocatalytic performance. The enhanced photocatalytic activity of BiOI/Bi_2WO_6 is attributable to the fact that the BiOI-sensitized Bi_2WO_6 exhibits increased surface area, a reduced band gap, enhanced absorption (at 380–600 nm) and inhibited recombination of photo-induced carriers [11]. Gui et al. [1] prepared WO_3/Bi_2WO_6 using a one-step hydrothermal method. The improved photocatalytic activity of WO_3/Bi_2WO_6 is attributed to its large surface area and low rate of recombination of photo-induced carriers. The photocatalytic activity of TiO_2/Bi_2WO_6 first increases and then declines as the TiO_2 loading increases, perhaps because of the reduction of the number of active sites as the TiO_2 content increases [12].

With respect to the doping of Bi_2WO_6 with a metal or a non-metal element, Cu loading effectively narrowed the band gap of Bi_2WO_6; moreover, the photocatalytic activity of Cu/Bi_2WO_6 followed the Cu loading order 7.5% > 10% > 0% > 2.5% > 20% [5]. Ren et al. [3] found that Ag loading improved charge separation, but very high Ag loading had the opposite effect, as it formed recombination centers, favoring the recombination of charge carriers, in a manner similar to that in Sn/Bi_2WO_6, as proposed by Kumar et al. [6]. The photocatalytic activity of Pt/Bi_2WO_6 followed the Pt loading order 0.8% > 1% > 0.5% > 1.5% > 0% [4]. Pt doping can promote interfacial charge transfer and inhibit the recombination of electron–hole pairs. The enhancement of the photocatalytic activity of nitrogen-doped Bi_2WO_6 is attributable to the reduction of electron–hole recombination and the increase in the transfer rate of photo-generated electrons to the surface of the photocatalyst [7]. Zhu et al. [10] revealed that nitrogen-doping improves the absorption of visible light by Bi_2WO_6. Zhang et al. [9] synthesized graphene/Bi_2WO_6 by the hydrothermal reduction and found that the high photocatalytic activity graphene/Bi_2WO_6 benefited from a synergetic effect of high adsorption, high light absorption and high electric conduction that is induced by the introduction of graphene. Fu et al. [8] utilized the hydrothermal method to generate boron-doped Bi_2WO_6 (B/Bi_2WO_6) and suggested that 0.5% B/Bi_2WO_6 exhibited the highest photocatalytic activity. Some boron atoms are located in the oxygen positions in the lattice, narrowing the band gap because the p-orbital of boron overlaps the p-orbital of oxygen [13]; other boron atoms are located at interstitial positions and act as electron traps; boron at both positions favors photocatalytic activity. In most related studies, the hydrothermal method is used to synthesize Bi_2WO_6 and to modify the photocatalytic activity of Bi_2WO_6. No investigation had been utilized solvothermal process to synthesize B/Bi_2WO_6; therefore, in this study, single-step solvothermal synthesis is used to generate B/Bi_2WO_6. In this study, the parent compound was C.I. Reactive Red 2 (RR2), which is a dye with the most commonly used anchor (the dichlorotriazine group). The objectives of this investigation are (1) to analyze the surface characteristics of B/Bi_2WO_6, (ii) to measure the photocatalytic activity of B/Bi_2WO_6 under irradiation by sunlight and visible light and (iii) to identify the major oxidative species in the B/Bi_2WO_6 system.

2. Materials and methods

2.1. Materials

Bismuth(III) nitrate ($Bi(NO_3)_3{\cdot}5H_2O$), sodium tungstate ($Na_2WO_4{\cdot}2H_2O$) and boric acid (H_3BO_3) were used as precursors in the formation of Bi, W and B, respectively, to generate Bi_2WO_6 and B/Bi_2WO_6 (Katayama, Japan). Ethylene glycol (EG) and sodium nitrite ($NaNO_2$) were used as a solvent in the solvothermal process and as an ultraviolent-light cut-off agent, respectively; both were obtained from Katayama. RR2 ($C_{19}H_{10}Cl_2N_6Na_2O_7S_2$) was purchased from Sigma-Aldrich (USA). To detect the active species that formed in the B/Bi_2WO_6 system, superoxide radicals, holes and hydroxyl radicals were detected by adding K_2CrO_4 (Katayama), ethylenediaminetetraacetic acid disodium salt (EDTA-2Na) (Katayama) and isopropanol (IPA) (J.T. Baker, USA), respectively. The solution pH was adjusted by adding 0.1 M HNO_3 or NaOH during the reaction and both of these reagents were purchased from Merck (USA). All chemicals were used without further purification and all solutions were prepared using deionized (DI) water (Milli-Q) and reagent-grade chemicals.

2.2. Preparations of Bi_2WO_6 and B/Bi_2WO_6

Bi_2WO_6 was prepared under the conditions that were identified as optimal by Wu et al. [14]. 1.319 g $Na_2WO_4{\cdot}2H_2O$, 3.881 g $Bi(NO_3)_3{\cdot}5H_2O$ and 0.062 g H_3BO_3 were added to 70 mL EG and the resulting solution was vigorously magnetically stirred. The B/W molar ratio was 0.25. The mixtures were adjusted to pH 2 using 10 M NaOH and stirring for 1 h. The mixtures were sealed in a 100 mL Teflon-lined stainless steel autoclave and heated at 433 K under self-generated pressure for 12 h, and then cooled naturally to room temperature. The precipitates were collected by filtration and washed using 50 mL 95% ethanol and 100 mL DI water to remove any residual impurities. The samples were finally dried in air at 333 K for 24 h. The obtained B/Bi_2WO_6 was denoted as BBW. When no boric acid was added, the obtained powder was pure Bi_2WO_6, denoted as BW.

2.3. Characterization of the photocatalysts

X-ray diffraction (XRD) patterns over the range $10° < 2\theta < 90°$ were used to analyze the phase components of BW and BBW samples (Bruker D8 SSS, Germany). The surface morphologies and microstructures of BBW were observed using a scanning electron microscope (SEM, JEOL 6330 TF, Japan) and a transmission electron microscope (TEM, JEOL 3010, Japan), respectively. Adsorption isotherms of N_2 on the prepared solids were measured at 77 K using a Micromeritica ASAP2020 apparatus (USA), and they were used to calculate the Brunauer-Emmett-Teller (BET) surface area. UV–Vis diffuse reflectance spectra of the samples over a wavelength range of 200–700 nm were obtained using a spectrophotometer (JAS.CO-V670, Japan). The surface charge of the samples in aqueous solution was measured using a zeta potential analyzer (BIC 90 plus, USA), and used to calculate the pH of the zero point of charge (pH_{zpc}). X-ray photoelectron spectroscopy (XPS) was used to elucidate the chemical states of the prepared photocatalysts, which were recorded using a PHI Quantum 5000 XPS system (USA) with a monochromatic Al Kα source

and a charge neutralizer. Binding energies were calibrated relative to the C_{1s} peak at 284.6 eV. Photoluminescence (PL) spectra were used to examine the efficiency of charge carrier transfer and separation because PL emission is caused by the recombination of photo-induced electron–hole pairs. The PL emission spectra of samples were obtained using a fluorescence spectrophotometer (Hitachi F-4500, Japan) at an excitation wavelength of 300 nm from a xenon lamp at room temperature.

2.4. Photodegradation experiments

Experiments were performed at pH 3 and 298 K. The RR2 concentration and photocatalyst dosage were 20 mg/L and 0.5 g/L, respectively, in all experiments. Adsorption experiments were conducted in darkness. In experiments in which scavengers were added, the initial molar concentration of each scavenger equaled the molar concentration of 0.5 g/L BBW. Photodegradation experiments were performed in a 3 L glass reactor. A 400 W Xe lamp (UniVex BT-580, Taiwan, 200 nm < wavelength < 700 nm) provided simulated sunlight. A quartz appliance that was filled with 2 M $NaNO_2$ solution was placed on the top of the reactor to cut the ultraviolet light and to provide visible light [15]. The reaction medium was stirred continuously at 300 rpm and aerated with air to maintain a suspension. Aliquots with a total volume of 10 mL were withdrawn from the photoreactor at predetermined intervals. Suspended photocatalyst particles were separated by filtration through a 0.22 μm filter (Millipore). The RR2 concentration was measured using a spectrophotometer (Hitachi U-5100, Japan) at 538 nm. Some experiments were conducted in triplicate and mean values were reported.

3. Results and discussion

3.1. Surface characteristics of photocatalysts

Fig. 1 shows the XRD patterns of BW and BBW. The peaks at 28.3°, 32.8°, 47.0°, 55.8°, 76.1° and 78.6° correspond to (1 1 3), (2 0 0), (0 2 6), (3 1 3), (3 3 3) and (2 4 0) of crystal phases, respectively. Both BW and BBW exhibit good crystallinity and their diffraction peaks correspond to the orthorhombic Bi_2WO_6 phase (JCPDS no. 73-1126). No other impurity, such as Bi_2O_3 or WO_3, was detected; moreover, no signal associated with boron was observed. Doping with boron did not significantly change the diffraction angles of BW. The crystalline sizes of BW and BBW were calculated from the XRD patterns using the Scherrer formula [16] (Eq. (1)):

$$D = \frac{k\lambda}{\beta\cos\theta} \quad (1)$$

where D represents the crystalline size in nm, λ is the X-ray wavelength (0.15418 nm), β is the line-width at half maximum of the peak at $2\theta = 28.3°$, k is the Scherrer constant (0.89) and θ is the diffraction angle (°). The calculated crystalline sizes of BW and BBW were 8.0 and 7.3 nm, respectively (Table 1), which were smaller than those of Bi_2WO_6 and B/Bi_2WO_6 that were formed by Fu et al. [8] using the hydrothermal method. Figs. 2(a) and (b) present SEM and TEM images of BBW, respectively, which reveals a high crystallinity, a high tendency to agglomerate and a thin sheet-shaped morphology with a length approximately 10 nm.

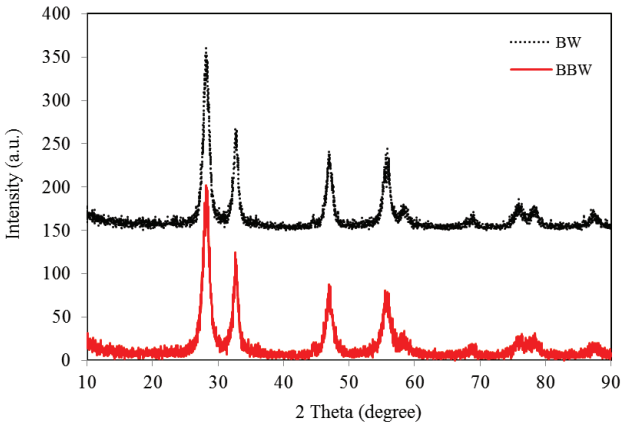

Fig. 1. XRD patterns of BW and BBW.

Table 1
Surface characteristics of BW and BBW

Characteristics	BW	BBW
BET surface area (m^2/g)	100.3	84.5
Pore volume (cm^3/g)	0.29	0.22
Band gap (eV)	3.1	3.1
Crystal size (nm)	8.0	7.3
pH_{zpc}	2.2	3.7

Table 1 lists the surface characteristics of BW and BBW. The BET surface area and pore volume of BW exceeded those of BBW; however, the pH_{zpc} of BW was less than that of BBW. Fu et al. [8] suggested that the BET surface area of B/Bi_2WO_6 declined slightly as the boron dopant content increased over 1%. The BET surface areas of BW and BBW were 100.3 and 84.5 m^2/g, respectively, and the corresponding pore volumes were 0.29 and 0.22 cm^3/g, respectively. In the investigation of Fu et al. [8], the BET surface areas of all samples were smaller than 12 m^2/g and the pore volumes were less than 0.1 cm^3/g. Despite the fact that the amount of boron doping (25%) herein exceeded that in Fu et al. [8], the BET surface area and pore volume of BBW obtained herein significantly exceeded those in Fu et al. [8]. The band gap of both BW and BBW was 3.1 eV. The absorption edge of photocatalysts is frequently extended by doping with impurities to narrow the band gap. The band gap is narrowed by the mixing of the boron p-orbital with the oxygen 2p-orbital, effectively inhibiting electron–hole recombination [17]. However, band gap narrowing did not occur in BBW in the present study. Wu et al. [18] indicated that substitutional boron atoms in the positions of oxygen atoms in TiO_2 form a narrow substitute band above the valence band. Fu et al. [8] found that doping Bi_2WO_6 with boron did not change its adsorption edge.

Fig. 3 shows the XPS spectra of BBW. Two of the peaks in the Bi_{4f} region (Fig. 3(a)) at 164.1 and 158.8 eV are attributed to $Bi_{4f5/2}$ and $Bi_{4f7/2}$, respectively [19–22], and are characteristic of Bi^{3+}. The binding energies of 37.2 and 35.0 eV for $W_{4f5/2}$ and $W_{4f7/2}$ can be assigned to the W^{6+} oxidation state (Fig. 3(b)) [20–22]. The O_{1s} region is associated with four peaks. The XPS spectral peaks at 529.9 and 531.7 eV in the O_{1s} region are attributed to Bi–O and W–O in Bi_2WO_6, respectively

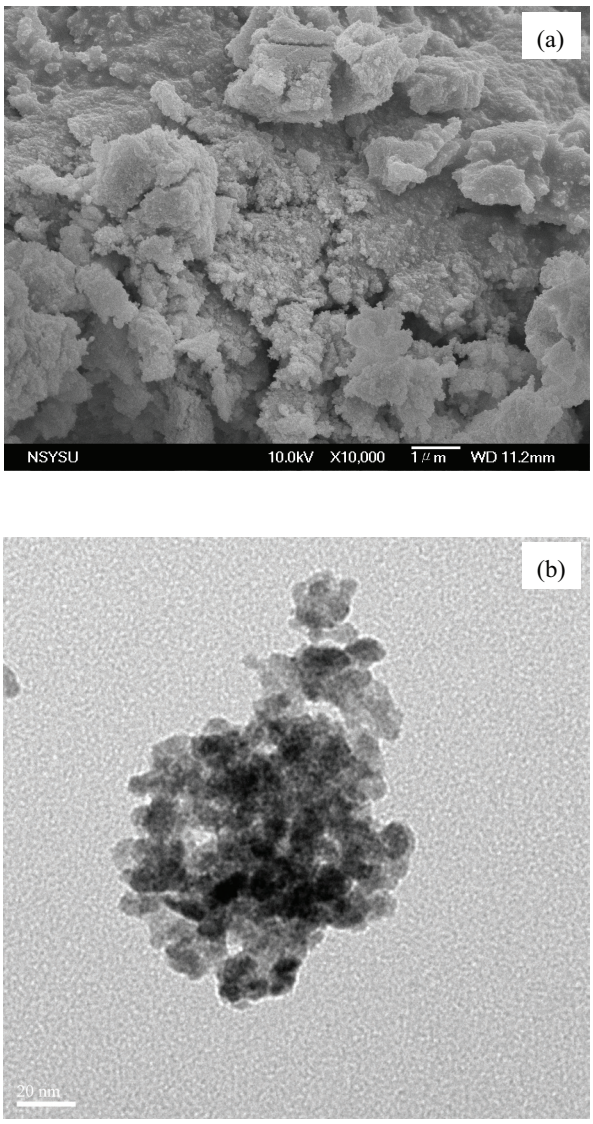

Fig. 2. Micrographs of BBW (a) SEM and (b) TEM.

(Fig. 3(c)) [23]. The peak at 531.1 eV indicates that hydroxyl groups (OH^-) were absorbed on the surface of BBW [22,24]. Based on the area analysis of fitted curves for BW (data not shown here) and BBW, the percentages of OH^- on the surfaces of BW and BBW in the O_{1s} region were 17.4% and 19.7%, respectively. BBW had more surface hydroxyl groups than BW, suggesting that the increase in the amount of surface hydroxyl groups may be the main cause of the enhancement in photocatalytic activity. Additionally, the hydroxyl groups effectively promote the trapping of photo-generated electrons by improving the surface adsorption of dissolved oxygen, and thereby inhibit the recombination of photo-generated electron–hole pairs [25]. The O_{1s} peak at 532.4 eV corresponds to B–O bonds in H_3BO_3 or B_2O_3 [26]. The peak at a binding energy of around 532 eV is associated with oxygen in the B–O–B bond [27]. BBW yielded two peaks in the B_{1s} region (Fig. 3(d)). Chen et al. [28] suggested that the binding energies of B_2O_3 and lattice boron were 193.5 and 188.5 eV, respectively. The binding energy of the B_{1s} core level in H_3BO_3 or B_2O_3 is centered at 193.0 eV (B–O bond) [26,27]. Therefore, the peak at 194.2 eV implies that B was present mainly as H_3BO_3 or B_2O_3 at the surface of BBW. However, the shift from 193.0 eV may also be indicative of a contribution by interstitial B [26]. Boron may be present both on the surface of and inside BW particles. Fu et al. [8] suggested that some boron atoms were doped into the O–W–O lattice, replacing some of the oxygen atoms that were originally bonded with W. Yang et al. [27] also showed that some boron dopant is embedded into the interstitial TiO_2 structure or incorporated into the TiO_2 lattice by occupying the positions of oxygen atoms. Hence, the binding energy of 188.7 eV (Fig. 3(d)) is suggested to be associated with the lattice boron that replaced oxygen atoms in the O–W–O lattice. For BBW, some of the boron dopant is embedded in the interstitial BW structure or incorporated into the BW lattice at the positions of oxygen atoms, whereas some is present as H_3BO_3 or B_2O_3 on the surface of BW. The B–O bond corresponds to 7.2% of the total area of the O_{1s} region (Fig. 3(c)), which is less than the theoretical doping amount (25%). Fu et al. [8] suggested that the actual amount of doping boron atoms may be lower than the theoretical value.

3.2. Determination of photocatalytic activity of photocatalysts

Fig. 4 shows the property of the adsorption and photodegradation of RR2 by BW and BBW. After 60 min of adsorption, BW and BBW had removed 17% and 33% of RR2, respectively. At pH 3, the surface charge of BW was negative (pH_{zpc} = 2.2) and that of BBW was positive (pH_{zpc} = 3.7). Since RR2 was an anionic dye in solution, the adsorption of RR2 by a positively charged surface was greater than that by a negatively charged surface. After 30 min of reaction, the removal of RR2 in sunlight/BW, visible light/BW, sunlight/BBW and visible-light/BBW systems was 82%, 19%, 93% and 88%, respectively. Under either sunlight or visible light, the photocatalytic activity of BBW exceeded that of BW. The adsorption of RR2 by BBW was high, and this high adsorption capacity of BBW is suggested to be responsible for its high photocatalytic efficiency in RR2 photodegradation. As in the work of Liu et al. [25], boron-doped BiOBr samples had a smaller surface area than pure BiOBr, and so adsorbed more dye, favoring photocatalytic activity.

The RR2 photodegradation rate constants (k) of the BW and BBW systems fitted pseudo-first-order kinetics, consistent with various studies of the photodegradation of dye [8,14,29]. Table 2 lists the k values of BW and BBW systems, which followed the order sunlight/BBW > visible-light/BBW > sunlight/BW > visible light/BW. One effect of doping BW with boron is to increase the amount of RR2 that undergoes reaction by increasing the adsorption capability of BW; another effect is the enhancement of the charge separation efficiency, which suppresses the recombination of electron–hole pairs (as discussed in relation to PL emission spectra); accordingly, the photocatalytic activity of BBW exceeded that of BW. Fu et al. [8] indicated that elemental boron is electron-deficient and oxytropic, so it can trap electrons, facilitating the separation of photo-generated electron–hole pairs, improving the photocatalytic activity of BW. In this study, the BET surface area, pore volume, band gap and photocatalytic activity of boron-doped Bi_2WO_6 following solvothermal synthesis herein all exceeded those following hydrothermal synthesis in Fu et al. [8]; however, the crystals were smaller.

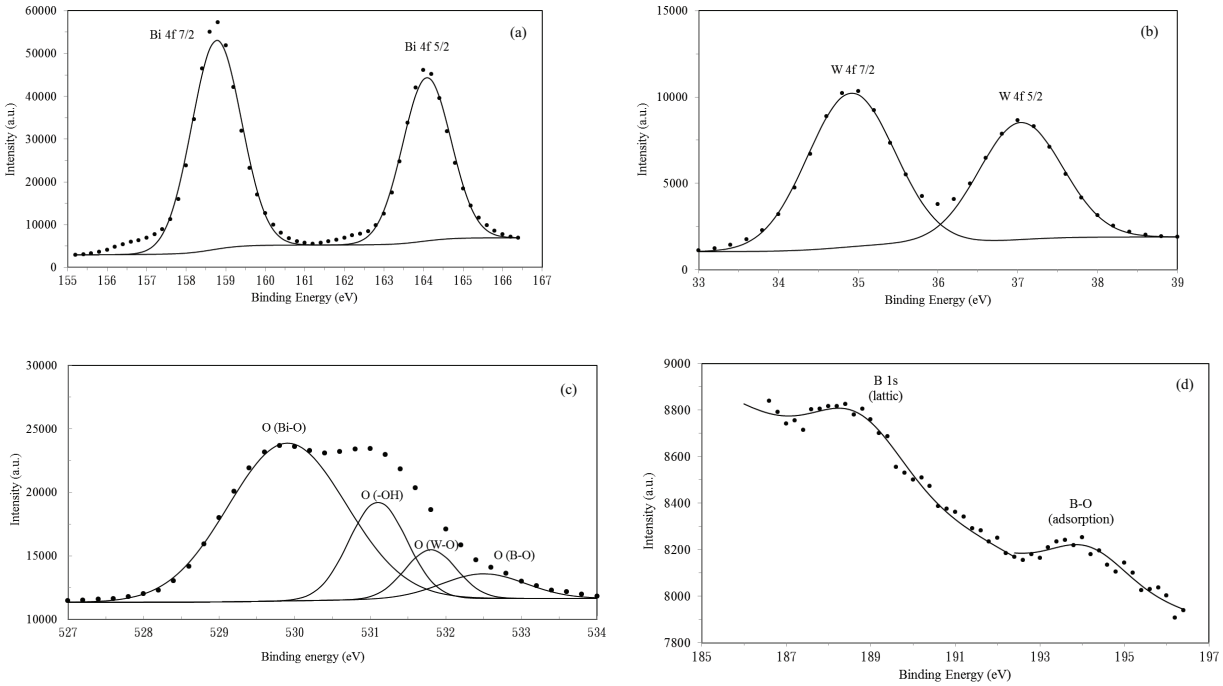

Fig. 3. XPS spectra of BBW for (a) Bi_{4f}, (b) W_{4f}, (c) O_{1s} and (d) B_{1s}.

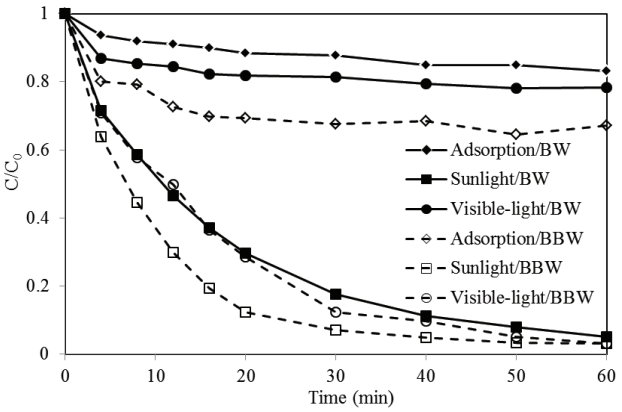

Fig. 4. Comparisons of photocatalytic activity of BW and BBW.

PL emission spectra are generated mainly by the recombination of photo-generated electron–hole pairs, so PL spectra are useful for evaluating the efficiency of separation of photo-generated electron–hole pairs in a photocatalyst [11]. Irradiating a photocatalyst causes electron–hole pair recombination, the emission of photons, and therefore PL. Generally, a lower PL intensity is associated with a lower rate of recombination of photo-generated electron–hole pairs and greater photocatalytic activity of the photocatalyst [7,11,30]. Fig. 5 presents PL spectra of BW and BBW in the range 400–550 nm. The strongest emission peak at 452 nm is attributed to the intrinsic luminescence of Bi_2WO_6, which originates from the charge-transfer transitions between the hybrid orbital of Bi_{6s} and O_{2p} (valence band) to the empty W_{5d} orbital (conduction band) in the WO_6^{2-} complex [31]. The emission peaks from BBW were much less intense, suggesting that the recombination of photo-generated electron–hole pairs was much lower in that compound. The fact that the PL intensity of BBW was lower than that of BW clearly reveals that the recombination of photo-generated charge carriers between the hybrid orbital of Bi_{6s} and O_{2p} to the empty W_{5d} orbital is greatly inhibited in BBW.

Table 2
Photocatalytic rate analysis of different systems

	k (h^{-1})	R^2
Sunlight/BW	3.34	0.999
Visible light/BW	0.14	0.898
Sunlight/BBW	6.19	0.998
Visible light/BBW	3.44	0.986
Sunlight/BBW/IPA	5.14	0.982
Sunlight/BBW/EDTA-2Na	0.13	0.934
Sunlight/BBW/Cr(VI)	3.46	0.979

The reusability of BBW was evaluated in three consecutive runs under irradiation by simulated sunlight. After the supernatant solution was removed by filtration, a fresh solution of 20 mg/L RR2 was added to begin the next run. Fig. 6 plots the cyclic photodegradation of RR2 in the sunlight/BBW system. The proportions of RR2 removed in runs 1, 2 and 3 were 97%, 86% and 63%, respectively. The photocatalytic activity of BBW declined over three cycles, probably because of the residual by-product of RR2 on the surface of BBW, which occupied some of the active sites of BBW. Hence, the photocatalytic activity of used BBW decreased. A future study should be performed to improve the stability of BBW during photocatalytic oxidation.

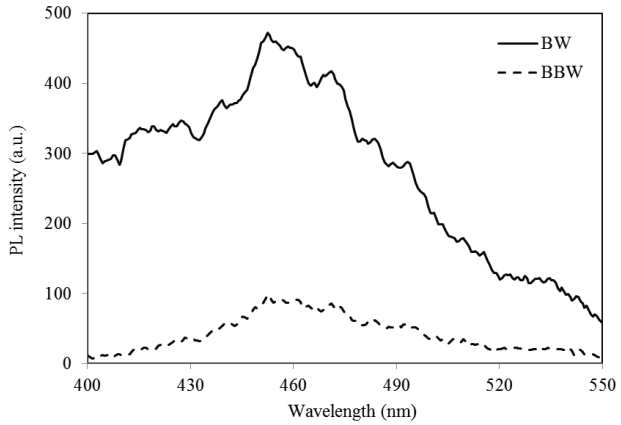

Fig. 5. PL spectra of BW and BBW.

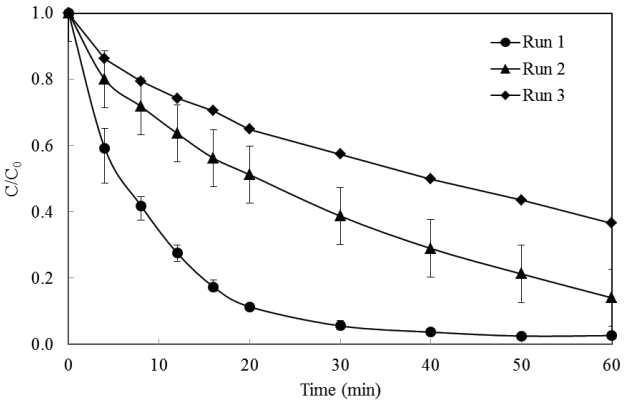

Fig. 6. Profiles of cyclic photodegradation for RR2 in sunlight/BBW system.

Organic matter can be oxidized directly by photo-generated holes, hydroxyl radicals that are formed by the oxidation of water with holes and other reactive oxygen species that are generated by electrons and dissolved oxygen [32]. To identify the active species in photodegradation herein, scavengers were added to the photodegradation system. Cr(VI) was used as the photo-generated electron scavenger to determine whether superoxide radicals were present. To trap radicals and holes, Cr(VI) [33,34], EDTA-2Na [19,35] and IPA [19,34,35] were utilized as superoxide radicals, holes and hydroxyl radical scavengers, respectively. Fig. 7 displays the degree of photodegradation of RR2 by sunlight/BBW in the presence of various scavengers. Adding IPA to the RR2 solution slightly reduced the rate of RR2 photodegradation but adding EDTA-2Na considerably slowed RR2 photodegradation (Table 2). In an aqueous photocatalytic reaction, photo-generated holes react with chemisorbed hydroxyl groups or water to form hydroxyl radicals and the photo-generated electrons interact with adsorbed oxygen to yield superoxide radicals, both of which are strongly oxidative species in the photodegradation of pollutants [20]. Photocatalytic reactions are well known to occur on or very near the surface of photocatalysts. Photo-generated holes were generated on the surface of BBW and cannot spread into the solution, indicating that improved adsorption promoted photodegradation by BBW.

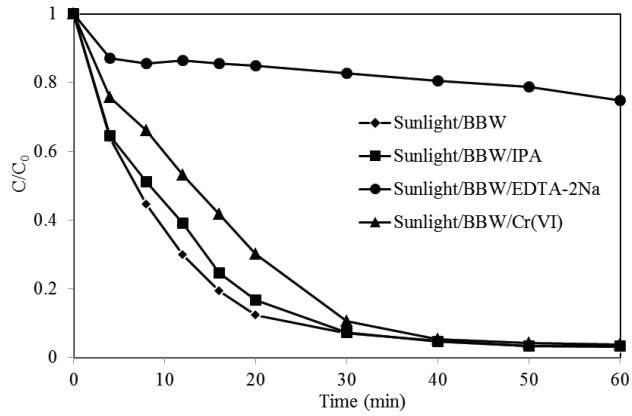

Fig. 7. Photodegradation of RR2 in sunlight/BBW system in the presence of different scavengers.

The photo-generated holes on the surface of BW did not react with OH^-/H_2O to form hydroxyl radicals [8,14]. Moreover, doping boron into BW did not change its band gap; accordingly, hydroxyl radicals were not thought to be produced in the BBW system. Photo-generated holes are suggested to have played a major role and superoxide radicals a minor role in the photodegradation of RR2 by BBW. Fu et al. [8] also claimed the photo-generated holes are the main active species that are responsible for photodegradation in B/Bi_2WO_6.

4. Conclusions

In this investigation, BBW was synthesized by doping boron into BW using a single-step solvothermal method. Doping with boron did not shift the light absorption region of BW. The BET surface area and pore volume of BW exceeded those of BBW; however, the pH_{zpc} of BW was smaller than that of BBW. In BBW, some boron dopant is embedded into the interstitial BW structure or incorporated into the BW lattice by occupying the positions of oxygen atoms, and the rest is present as H_3BO_3 or B_2O_3 on the surface of BW. The doping boron acted as electron traps and thereby facilitated the separation of photo-generated electron–hole pairs, improving photocatalytic activity. This study suggested that photo-generated holes and superoxide radicals, rather than hydroxyl radicals, dominated the degradation of RR2 by BBW in sunlight.

Acknowledgment

The authors would like to thank the National Science Council of the Republic of China, Taiwan, for financially supporting this research under Contract No. MOST 105-2221-E-151-001.

References

[1] M.S. Gui, W.D. Zhang, Y.Q. Chang, Y.X. Yu, One-step hydrothermal preparation strategy for nanostructured WO_3/Bi_2WO_6 heterojunction with high visible light photocatalytic activity, Chem. Eng. J., 197 (2012) 283–288.

[2] P. Ju, P. Wang, B. Li, H. Fan, S. Ai, D. Zhang, Y. Wang, A novel calcined $Bi_2WO_6/BiVO_4$ heterojunction photocatalyst with highly enhanced photocatalytic activity, Chem. Eng. J., 236 (2014) 430–437.

[3] J. Ren, W. Wang, S. Sun, L. Zhang, J. Chang, Enhanced photocatalytic activity of Bi_2WO_6 loaded with Ag nanoparticles under visible light irradiation, Appl. Catal., B, 92 (2009) 50–55.
[4] F. Duan, Y. Zheng, M. Chen, Flowerlike $PtCl_4/Bi_2WO_6$ composite photocatalyst with enhanced visible-light-induced photocatalytic activity, Appl. Surf. Sci., 257 (2011) 1972–1978.
[5] G. Tan, J. Huang, L. Zhang, H. Ren, A. Xia, An enhanced visible-light-driven photocatalyst: conduction band control of Bi_2WO_6 crystallites by Cu ion modification, Ceram. Int., 40 (2014) 11671–11679.
[6] B.V. Kumar, M.D. Prasad, M. Vithal, Enhanced visible light photocatalytic activity of Sn doped Bi_2WO_6 nanocrystals, Mater. Lett., 152 (2015) 200–202.
[7] M. Shang, W. Wang, L. Zhang, H. Xu, Bi_2WO_6 with significantly enhanced photocatalytic activities by nitrogen doping, Mater. Chem. Phys., 120 (2010) 155–159.
[8] Y. Fu, C. Chang, P. Chen, X. Chu, L. Zhu, Enhanced photocatalytic performance of boron doped Bi_2WO_6 nanosheets under simulated solar light irradiation, J. Hazard. Mater., 254–255 (2013) 185–192.
[9] J. Zhang, Z.H. Huang, Y. Xu, F. Kang, Hydrothermal synthesis of graphene/Bi_2WO_6 composite with high adsorptivity and photoactivity for azo dyes, J. Am. Ceram. Soc., 96 (2013) 1562–1569.
[10] G. Zhu, J. Liang, M. Hojamberdiev, S.A. Bilmes, X. Wei, P. Liu, J. Zhou, Ethylenediamine (EDA) – assisted hydrothermal synthesis of nitrogen-doped Bi_2WO_6 powders, Mater. Lett., 122 (2014) 216–219.
[11] H. Li, Y. Cui, W. Hong, High photocatalytic performance of BiOI/Bi_2WO_6 toward toluene and Reactive Brilliant Red, Appl. Surf. Sci., 264 (2013) 581–588.
[12] J. Li, Z. Guo, Y. Wang, Z. Zhu, Three-dimensional TiO_2/Bi_2WO_6 hierarchical heterostructure with enhanced visible photocatalytic activity, IET Micro Nano Lett., 9 (2014) 65–68.
[13] A. Zaleska, E. Grabowska, J.W. Sobczak, M. Gazda, J. Hupka, Photocatalytic activity of boron-modified TiO_2 under visible light: the effect of boron content, calcination temperature and TiO_2 matrix, Appl. Catal., B, 89 (2009) 469–475.
[14] C.H. Wu, C.Y. Kuo, J.T. Wu, M.J. Hsu, T.J. Jhang, Photodegradation of C.I. Reactive Red 2 in the Bi_2WO_6 system: determination of surface characteristics and photocatalytic activities of Bi_2WO_6, React. Kinet. Mech. Catal., 117 (2016) 391–404.
[15] M. Su, C. He, V.K. Sharma, M.A. Asi, D. Xia, X.Z. Li, H. Deng, Y. Xiong, Mesoporous zinc ferrite: synthesis, characterization, and photocatalytic activity with H_2O_2/visible light, J. Hazard. Mater., 211–212 (2012) 95–103.
[16] P. Klug, L.E. Alexander, X-ray Diffraction Procedures, Wiley, New York, 1974.
[17] B. Wang, X.Y. Lu, J. Xuan, K.H. Leung, Facile synthesis and photocatalytic disinfection of boron self-doped TiO_2 nanosheets, Mater. Lett., 115 (2014) 57–59.
[18] Y.M. Wu, M.Y. Xing, J.L. Zhang, Gel-hydrothermal synthesis of carbon and boron co-doped TiO_2 and evaluating its photocatalytic activity, J. Hazard. Mater., 192 (2011) 368–373.
[19] M.S. Gui, W.D. Zhang, Q.X. Su, C.H. Chen, Preparation and visible light photocatalytic activity of Bi_2O_3/Bi_2WO_6 heterojunction photocatalysts, J. Solid State Chem., 184 (2011) 1977–1982.
[20] Z. Zhang, W. Wang, E. Gao, M. Shang, J. Xu, Enhanced photocatalytic activity of Bi_2WO_6 with oxygen vacancies by zirconium doping, J. Hazard. Mater., 196 (2011) 255–262.
[21] Y. Guo, G. Zhang, H. Gan, Synthesis, characterization and visible light photocatalytic properties of Bi_2WO_6/rectorite composites, J. Colloid Interface Sci., 369 (2012) 323–329.
[22] Z. Sun, X. Li, S. Guo, H. Wang, Z. Wu, One-step synthesis of Cl^--doped Pt(IV)/Bi_2WO_6 with advanced visible-light photocatalytic activity for toluene degradation in air, J. Colloid Interface Sci., 412 (2013) 31–38.
[23] M.S. Gui, W.D. Zhang, Preparation and modification of hierarchical nanostructured Bi_2WO_6 with high visible light-induced photocatalytic activity, Nanotechnology, 22 (2011) 265601.
[24] S. Bai, H. Liu, J. Sun, Y. Tian, S. Chen, J. Song, R. Luo, D. Li, A. Chen, C.C. Liu, Improvement of TiO_2 photocatalytic properties under visible light by WO_3/TiO_2 and MoO_3/TiO_2 composites, Appl. Surf. Sci., 338 (2015) 61–68.
[25] Z.S. Liu, J.L. Liu, H.Y. Wang, G. Cao, J.N. Niu, Boron-doped bismuth oxybromide microspheres with enhanced surface hydroxyl groups: synthesis, characterization and dramatic photocatalytic activity, J. Colloid Interface Sci., 463 (2016) 324–331.
[26] D.H. Quinones, A. Rey, P.M. Alvarez, F.J. Beltran, G.L. Puma, Boron doped TiO_2 catalysts for photocatalytic ozonation of aqueous mixtures of common pesticides: diuron, o-phenylphenol, MCPA and terbuthylazine, Appl. Catal., B, 178 (2015) 74–81.
[27] H. Yang, Y. Wang, X. Xue, Influences of glycerol as an efficient doping agent on crystal structure and antibacterial activity of B-TiO_2 nano-materials, Colloids Surf., B, 122 (2014) 701–708.
[28] L. Chen, T. Goto, T. Hiral, State of boron in chemical vapour-deposited SiC-B composite powders, J. Mater. Sci. Lett., 9 (1990) 997–999.
[29] C.Y. Kuo, C.H. Wu, S.T. Chen, Decolorization of C.I. Reactive Red 2 by UV/TiO_2/PAC and visible light/TiO_2/PAC systems, Desal. Wat. Treat., 52 (2014) 834–843.
[30] L.Q. Jing, Y.C. Qu, B.Q. Wang, S.D. Li, B.J. Jiang, L.B. Yang, W. Fu, H.G. Fu, J.Z. Sun, Review of photoluminescence performance of nano-sized semiconductor materials and its relationships with photocatalytic activity, Sol. Energy Mater. Sol. Cells, 90 (2006) 1773–1787.
[31] Q. Xiao, J. Zhang, C. Xiao, X. Tan, Photocatalytic degradation of methylene blue over Co_3O_4/Bi_2WO_6 composite under visible light irradiation, Catal. Commun., 9 (2008) 1247–1253.
[32] S. Garcia-Segura, E. Brillas, Applied photoelectrocatalysis on the degradation of organic pollutants in wastewaters, J. Photochem. Photobiol., C, 31 (2017) 1–35.
[33] Y. Chen, S. Yang, K. Wang, L. Lou, Role of primary active species and TiO_2 surface characteristic in UV-illuminated photodegradation of Acid Orange 7, J. Photochem. Photobiol., A, 172 (2005) 47–54.
[34] Y. Zhang, C. Shao, X.H. Li, N. Lu, M.Y. Zhang, P. Zhang, X. Zhang, Y. Liu, Controllable synthesis and enhanced visible photocatalytic degradation performances of Bi_2WO_6–carbon nanofibers heteroarchitectures, J. Sol-Gel Sci. Technol., 70 (2014) 149–158.
[35] H. Huang, K. Liu, K. Chen, Y. Zhang, Y. Zhang, S. Wang, Ce and F comodification on the crystal structure and enhanced photocatalytic activity of Bi_2WO_6 photocatalyst under visible light irradiation, J. Phys. Chem. C, 118 (2014) 14379–14387.